OPTOELECTRONICS AND ADVANCED MATERIALS – RAPID COMMUNICATIONS Vol. 13, Iss. 1-2, January-February 2019, p. 104 - 110

Thickness dependence of microstructures and optical properties of $Mn_{1.56}Co_{0.96}Ni_{0.48}O_4$ thin films

CHAO MA[a,*], WEI REN[b], LEI WANG[c]
[a]College of Electronic Engineering, Chengdu Technological University, Chengdu 611730, China
[b]School of Science, Xi'an University of Posts and Telecommunications, Xi'an 710121, China
[c]School of Environmental Science & Engineering, Shanghai Jiao Tong University, Shanghai 200240, China

$Mn_{1.56}Co_{0.96}Ni_{0.48}O_4$ (MCN) thin films with different thicknesses were synthesized on Si substrates by the chemical solution deposition method. Microstructures of the thin films were determined by atomic force microscopy. The ion-by-ion growth mechanism was the main reason for the grain size increased with the increasing film thickness. The refractive indices and extinction coefficients of MCN thin films were determined by measuring ellipsometry parameters and modeled through the Tauc-Lorentz oscillator dispersion formula in the wavelength range of 280–850 nm. The optical constants *n* and *k* of MCN thin films were found to decrease with increasing thickness due to the variations in microstructures.

(Received April 18, 2018; accepted February 12, 2019)

Keywords: Thin film, Thickness dependence, Microstructure, Optical property

1. Introduction

Transition metal oxides have been applied in numerous applications, such as high-temperature superconductivity, colossal magnetoresistance, photodetectors, thermistors and so on [1, 2]. As representatives of transition metal oxide thermistors, Mn-Co-Ni-O spinels with the general formula AB_2O_4 have been widely used as bolometers and uncooled infrared detectors [3-5]. These oxides exhibit negative temperature coefficient characteristics and have moderate resistivities and high temperature coefficients of resistance (*B* values) [6]. In addition, they have a broad spectral response due to the strong coupling to the external electromagnetic waves which generated from the high polarizability between transition metals and oxides [7]. It is known that the resistivity can be controlled by altering the relative content of the metal species, thereby producing a series of solid solutions. $Mn_{1.56}Co_{0.96}Ni_{0.48}O_4$ (MCN) becomes an especially important composition because it is very close to the minimum resistivity in these ternary oxides [8]. Dense polycrystalline MCN thin films exhibit good crystallization and electrical properties, such as low resistance, high sensitivity and stability, compared to their bulk counterparts. Additionally, MCN and its complexed thin films have relatively large absorption coefficients and can be promising candidates for the electrode and thermal absorption layers in detectors [9, 10]. Although MCN thin film has been utilized in oxide optoelectronics for a long time, there are still many aspects remaining unclear.

Many researchers have pointed out that the optical properties of MCN thin films were depending on the microstructure, stoichiometry, annealing temperature, ambient temperature and so on [11-13]. YQ Gao have compared the optical properties of the amorphous and crystalline MCN thin films, and attributed the critical points appear in the optical constant spectra to annealing temperature effects on the change in the film structures [14]. W Zhou have reported that the infrared optical properties of $Mn_{1.4}Co_{1.0}Ni_{0.6}O_4$ thin films grown by the post-annealed process could be affected by the oxidation states of the films [15]. Moreover, the thickness dependence of optical property of MCN thin film is also an important aspect to be considered when developing practical applications. In this work, we investigated the effect of thickness variation on the microstructures and optical properties of MCN thin films.

2. Experimental

MCN thin films were synthesized on crystalline Si (100) substrates by the chemical solution deposition (CSD) method. $Mn(CH_3COO)_2 \cdot 4H_2O$ (AR, 99%), $Co(CH_3COO)_2 \cdot 4H_2O$ (AR, 99%), and $Ni(CH_3COO)_2 \cdot 4H_2O$ (AR, 99%) were used as the raw materials with the cation stoichiometric ratio of Mn: Co: Ni at 13: 8: 4. These acetates were first dissolved in glacial acetic acid and the concentration of the precursor solution was adjusted to 0.2 M. The solution was filtered through a 0.45 μm syringe filter to avoid particulate contamination. The filtering step was followed by spin-coating the solutions at 3000 rpm for 20 s to form a

wet film on Si substrate. The spin coated substrate was then dried at 350 °C for 5 minutes. The spin coating and heat-treatment procedures were repeated 6, 8 and 9 times, to form three sets of films with increasing thickness labeled as S1, S2 and S3, respectively. The resulting films were finally annealed at 750 °C for 1 h in air to improve the crystallinity.

Crystallization properties and surface morphology of the samples were investigated by X-ray diffraction (XRD, Bruker D8) and atomic force microscopy (AFM, Asylum Research MFP-3DTM). Cross-sectional images and chemistry of the thin films were obtained using scanning electron microscopy (SEM, Supra55VP, Zeiss) equipped with energy dispersive X-ray spectroscopy (EDS). The elemental analyses were characterized by X-ray photoelectron spectroscopy (XPS, Shimadzu AXIS-ULTRA DLD) with Al Kα radiation ($h\nu$=1486.6 eV). Optical characteristics of the films were obtained by spectroscopic ellipsometry (SENTECH SE850) at room temperature in the wavelength range of 280–850 nm and at an incident angle of 70°.

3. Results and discussion

Fig. 1 shows the XRD patterns of three samples deposited on Si substrates (the peaks of Si (400) are located at about 70° and not shown here). All diffraction peaks are assigned to the spinel structure with a space group of Fd-3m (according to JCPDS-ICDD 84-0542), and the strong and narrow diffraction peaks indicate that the well crystallized polycrystalline films have been obtained. It can also be observed that the strength of the peaks increases with increasing film thickness, especially in (311) and (400) directions. Crystallite sizes are approximately calculated by the Scherrer equation and obtained as 27.3, 29.8 and 32.3 nm for S1, S2 and S3, respectively. This result is consistent with previous studies that the crystallite size increases with increasing the film thickness [16].

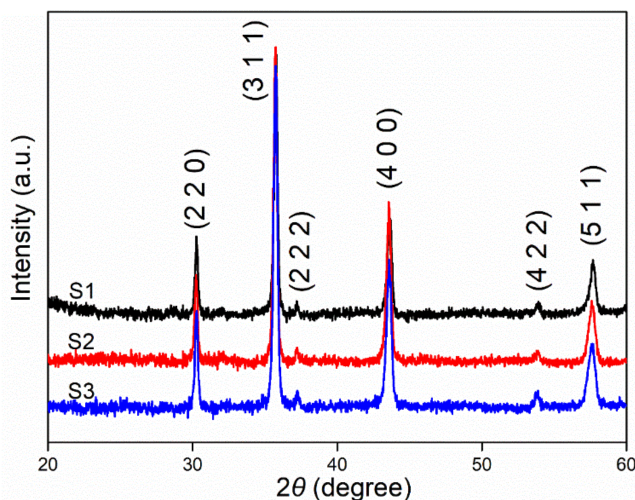

Fig. 1. XRD patterns of MCN thin films

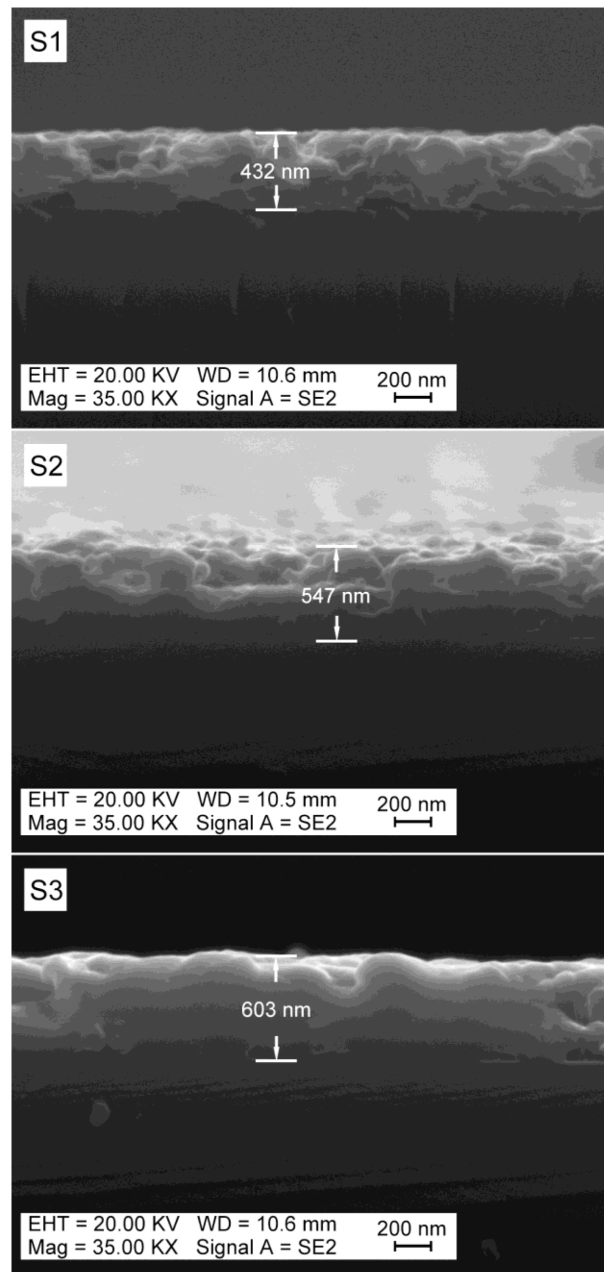

Fig. 2. Cross-sectional SEM images of MCN thin films

Fig. 2 shows the film thicknesses determined by cross-sectional morphologies obtained by SEM. The thicknesses of S1, S2 and S3 samples are found to be 432 nm, 547 nm and 603 nm, respectively. According to EDS measurements, the constituent elements of all samples are present at the expected levels. The atomic percent results for the three samples are shown in Table 1.

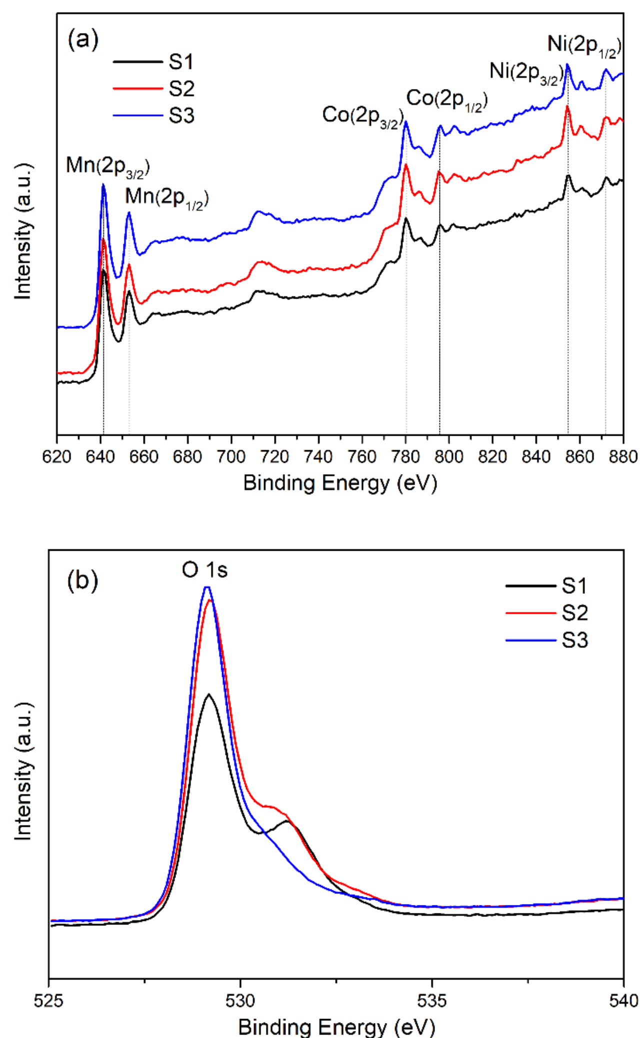

Fig. 3. XPS spectra of (a) Mn 2p, Co 2p, Ni 2p and (b) O 1s of MCN thin films

The XPS analysis is further performed to investigate the surface chemical environment of the three samples. The results of XPS for MCN thin films are presented in Fig. 3. The peaks observed at 641.0, 653.1, 780.5, 796.1, 854.3 and 871.7 eV correspond to Mn $2p_{3/2}$, Mn $2p_{1/2}$, Co $2p_{3/2}$, Co $2p_{1/2}$, Ni $2p_{3/2}$ and Ni $2p_{1/2}$, respectively [17, 18]. The Mn 2p spectra of three samples do not contain any shake-up feature at higher binding energy, suggesting the absence of Mn^{2+} [15]. Two distinguishable satellite peaks at 786 and 802 eV above the Co $2p_{3/2}$ and Co $2p_{1/2}$ mean that there only Co^{2+} exists in the thin films [18]. The most intense peak of Ni $2p_{3/2}$ located at about 854.3 eV and the shake-up feature of Ni $2p_{1/2}$ at above 871.7 eV confirm that the presence of Ni^{2+} [19]. The O 1s spectra exhibit the major components centered at 529.1 eV, which can be attributed to the bonds between oxygen and metal ions [20]. It can be clearly seen that the thickness increase results in an observable increase of the intensity of peak with the position remain unchanged. This confirms that more cations are oxidized as the thickness increases.

Table 1. Atomic percentages of MCN thin films

Sample	Elemental % (Atom.)		
	Mn	Co	Ni
S1	50.48	31.76	17.76
S2	51.03	31.70	17.27
S3	51.95	31.67	16.38

AFM images of MCN thin films are shown in Fig. 4. The surface roughness values of three thin films measured by AFM are 8.5, 4.5 and 9.1 nm, corresponding to S1, S2, and S3, respectively. It is evident that the grain size is a function of the film thickness, and the grain size increases as the film thickness increases.

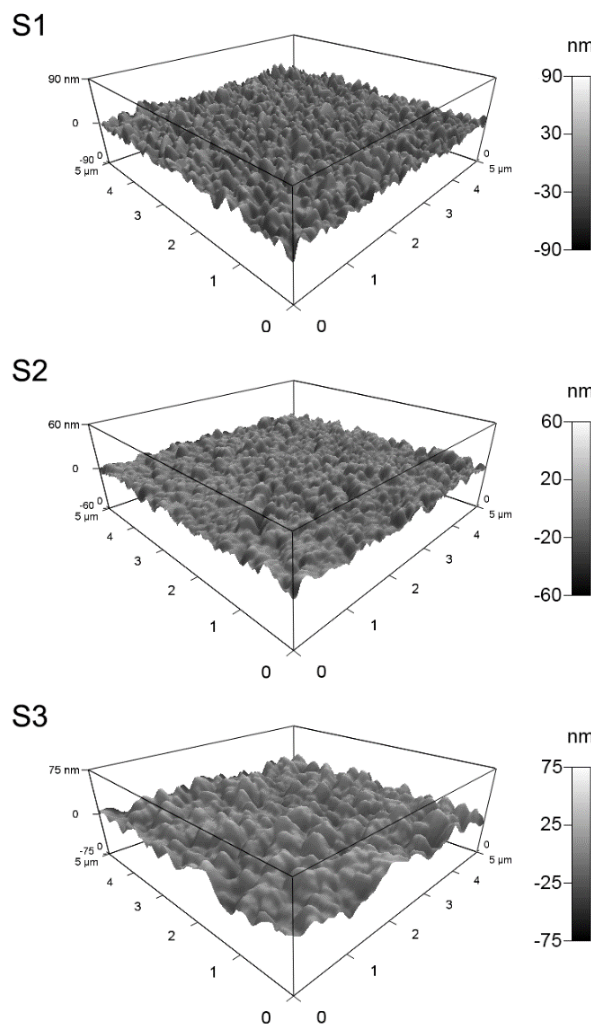

Fig. 4. AFM images of MCN thin films

A two-step process is employed in this work to accomplish the conversion of the as-deposited film into

the crystalline state. In this approach, the removal of organic constituents is carried out in a separate processing step (i.e., the first stage of the two-step method) at lower temperatures (350 °C) prior to a high-temperature crystallization step (750 °C). The as-deposited film can be first considered as an ion-by-ion network based on a homogeneous particle-free solution in a high degree of supersaturation [21]. During the conversion, these clusters first rearrange to form an inorganic amorphous film, which then transforms to the MCN film by nucleation and growth processes [22]. Cross-sectional SEM images also confirm that MCN thin films crystallize with columnar microstructures, similar to the mechanism observed in PZT films [23]. The nucleation of the spinel phase occurring at the substrate interface and the grain growth from these nuclei appears to proceed towards the surface of the film. Hence, for this type of nucleation and growth behavior, it is likely that crystal growth occurs on nuclei already present on the substrate and the crystal size can increase with increasing deposition [21]. Naturally, the grain size increases with increasing film thickness.

Spectroscopic ellipsometry is a contactless and nondestructive optical technique. It deals with the amplitude Ψ and phase Δ of the complex reflectance ratio ρ of the p (parallel) and s (perpendicular) field components of the light beam defined with respect to the plane of incidence of the sample [12]:

$$\rho = \frac{R_p}{R_s} = \tan\Psi \exp(i\Delta) \qquad (1)$$

where R_p and R_s are the complex reflection coefficients of the light polarized parallel and perpendicular to the plane of incidence, respectively. The ellipsometry parameters Ψ and Δ are ellipsometry angles. The tanΨ gives the ratio between the absolute values of these two electric field components and Δ represents the phase difference between them.

To estimate the optical constants of the MCN thin films, a four-layer model (air/surface roughness layer/thin film/Si substrate) is built and the parameters are varied to obtain a best fit to the measured parameters Ψ and Δ. The Si layer is thick enough that the light cannot propagate through it. The optical constants of Si are based on the parameters of the Si (100) standard sample and are obtained by ellipsometry software (SpectraRay/3). Fig. 5 shows the measured and fitted ellipsometry spectra of MCN thin films at the wavelength range of 280-850 nm. The measured ellipsometry parameters are fitted by Tauc-Lorentz (TL) oscillator dispersion formula. The experimental and calculated spectra of Ψ and Δ are fitted each other. Thus, it can be verified that the fitting model used is adequate to describe the dispersion of the optical properties of MCN thin films in the measured wavelength ranges. The corresponding fitting parameters of MCN thin films are listed in Table 2.

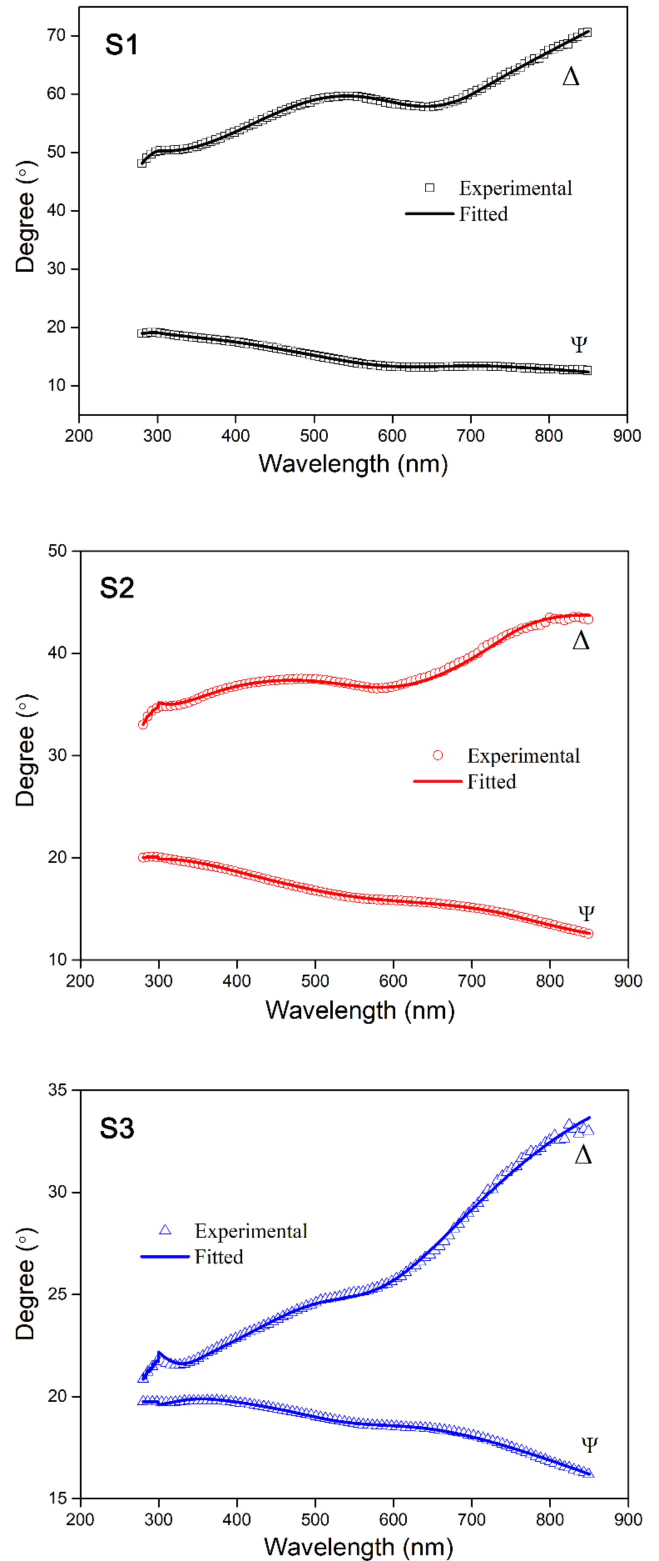

Fig. 5. Experimental (symbols) and fitted (solid lines) ellipsometry spectra of Ψ and Δ of MCN thin films

Table 2. Fitting parameters of MCN thin films

Sample		**S1**	**S2**	**S3**
Surface roughness layer	Thickness (nm)	9.6	6.3	11.2
	Fraction of inclusion	0.5	0.5	0.5
MCN layer	E_g (0)	0.95	0.89	0.84
	A (0)	-108.99	-106.96	-105.59
	E_0 (0)	4.62	4.09	3.32
	C (0)	9.30	5.68	5.45
	E_g (1)	0.89	0.49	0.45
	A (1)	90.01	88.95	82.95
	E_0 (1)	6.21	5.75	5.36
	C (1)	11.04	12.92	14.67
	E_g (2)	1.75	1.49	0.97
	A (2)	30.58	44.76	51.23
	E_0 (2)	1.98	2.56	3.08
	C (2)	1.60	2.98	4.08

The TL oscillator dispersion formula is used to model a dielectric function for film properties. The TL dispersion function can be expressed as [24]:

$$\varepsilon_2(E) = \begin{cases} \dfrac{AE_nC(E-E_g)^2}{(E^2-E_n^2)^2+C^2E^2}\dfrac{1}{E} & (E > E_g) \\ 0 & (E \le E_g) \end{cases} \qquad (2)$$

where A is the oscillator strength, E_n is the peak transition energy, C is the broadening term, and E_g is the band gap energy. The real part ε_1 of the TL model is the result of self-consistent Kramers–Kronig integration of ε_2:

$$\varepsilon_1 = \varepsilon_\infty + \frac{2}{\pi}P\int_{E_g}^{\infty}\frac{\xi\varepsilon_2(E)}{\xi^2-E^2}d\xi \qquad (3)$$

where ε_∞ is the high frequency dielectric constant, P is the principal value of the integral. Meanwhile, the optical constants (the refractive index n and extinction coefficient k) are determined as follows:

$$n = \frac{1}{\sqrt{2}}\sqrt{\sqrt{\varepsilon_1^2+\varepsilon_2^2}+\varepsilon_1}$$
$$k = \frac{1}{\sqrt{2}}\sqrt{\sqrt{\varepsilon_1^2+\varepsilon_2^2}-\varepsilon_1} \qquad (4)$$

From the best fit obtained between the measured and fitted data, the evaluated optical constants of the MCN thin films are presented in Fig. 6. The refractive indices of three samples generally increase with increasing wavelength, as shown in Fig. 6 (a). Anomalous dispersion occurs in the entire wavelength range, where the frequency of the light is close to the absorption resonance of the films. The n values of MCN thin films are observed to decrease with increasing thickness. It should be noted that the resonant oscillation of the electric polarization occurs in the UV/visible wavelength band, and the refractive index is essentially determined by the electric polarization and is proportional to the electric polarization [25]. We hypothesize that the polarization profile of three samples is strongly dependent on the film thickness, and it becomes more inhomogeneous due to the smaller grain size in the thinner films [26, 27]. Therefore, the decreased refractive index of MCN thin films could be primarily attributed to the weakening of the polarization due to the increased grain size in thicker films.

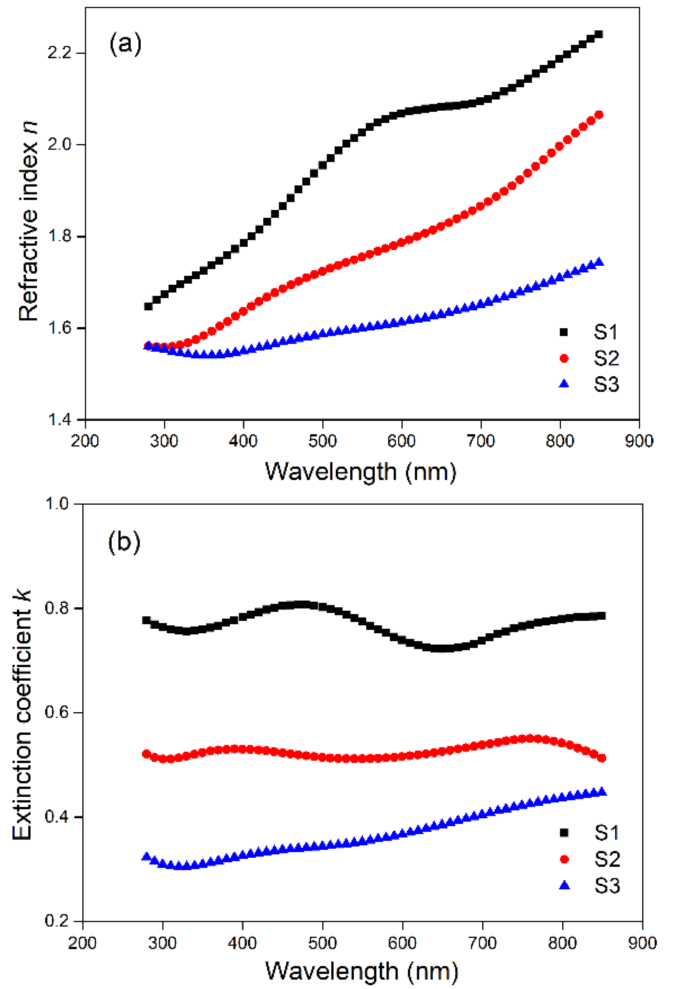

Fig. 6. (a) Refractive index n and (b) extinction coefficient k of MCN thin films

The k values of MCN thin films also decrease with increasing thickness. The extinction coefficient in this case is derived from a combination of absorption and scattering processes [28]. Smaller grain size indicates that more grain boundaries, which leads to the enhanced interaction between the film surface and the incident light [29]. Hence, longer path lengths result in higher

absorption. In addition, due to the characteristics of the ion-by-ion mechanism for MCN films prepared by the CSD method, the thin films are highly scattering, and this scattering increases as film thickness decreases [21]. Combined with these two factors, the decrease in the extinction coefficient with increasing thickness of MCN thin films can be explained.

The absorption coefficient α of the films as a function of wavelength is expressed as

$$\alpha = \frac{4\pi k}{\lambda} \quad (5)$$

where λ is the wavelength of the light and k is the extinction coefficient. The absorption coefficient peaked at approximately 2.15×10^5, 1.38×10^5 and 0.91×10^5 cm^{-1} at 472 nm for S1, S2 and S3, respectively.

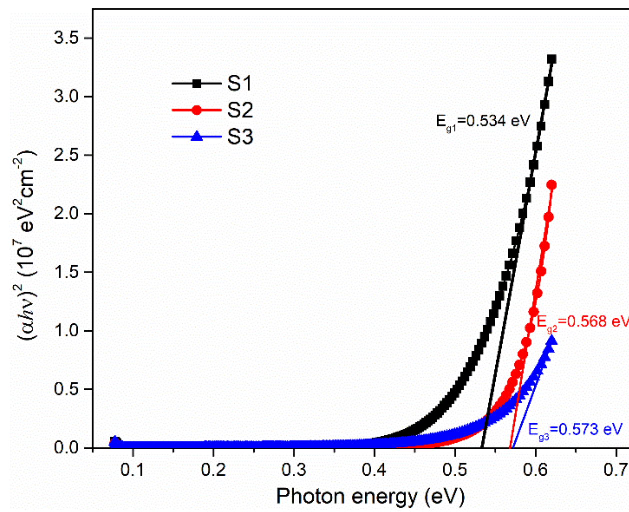

Fig. 7. Plots of $(\alpha h\nu)^2$ versus photon energy for MCN thin films

The energy gap E_g of MCN thin film can be determined by assuming a direct transition between valence and conduction bands [30]. The relation between the energy gap E_g and absorption coefficient α is given by the Tauc equation

$$(\alpha h\nu)^2 = A(h\nu - E_g) \quad (6)$$

where $h\nu$ is the incident photon energy and A is a constant which does not depend on photon energy. The $(\alpha h\nu)^2$ versus E curves for the MCN thin films are shown in Fig. 7. The values of E_g estimated from the graph, by extrapolating the linear portions of the plots to $(\alpha h\nu)^2 = 0$, are 0.534, 0.568 and 0.573 eV for S1, S2 and S3, respectively. The band gap energy values of MCN thin films are consistent with previous reports [30].

4. Conclusions

In summary, the crystallinity, microstructure and optical properties of MCN thin films with different thicknesses are studied by XRD, SEM, EDS, XPS, AFM and spectroscopic ellipsometry techniques. The grain size of the thin films increases monotonously with increasing thickness due to the ion-by-ion growth mechanism. The optical constants of MCN thin films in the visible wavelength range decrease with increasing thickness, primarily due to the increase in grain size. The S1 sample with smallest grain size will exhibit excellent optical properties in the low light loss applications in the visible wavelength range due to its large reflective index value and strong optical absorption. Therefore, it is feasible to fabricate an MCN thin film with controllable texture and microstructure, and to develop an electro-optic thin film with higher performance.

Acknowledgments

This work was supported by the National Natural Science Foundation of China (No. 61504168), the Research Project of the Introduction Talent (No. 2017RC015).

References

[1] C. N. R. Rao, Annu. Rev. Phys. Chem. **40**(1), 291 (1989).

[2] Z. Sun, T. Liao, Y. Dou, S. M. Hwang, M. S. Park, L. Jiang, J. H. Kim, S. X. Dou, Nat. Commun. **5**(10), 3813 (2014).

[3] S. W. Ko, H. M. Schulze, D. B. Saint John, N. J. Podraza, E. C. Dickey, S. S. Trolier-McKinstry, J. Am. Ceram. Soc. **95**(8), 2562 (2012).

[4] A. Feteira, J. Am. Ceram. Soc. **92**(5), 967 (2009).

[5] K. Park, D. Y. Bang, J. Mater. Sci. Mater. Electron. **14**(2), 81 (2003).

[6] K. Park, J. Am. Ceram. Soc. **88**(4), 862 (2005).

[7] Z. M. Huang, W. Zhou, C. Ouyang, J. Wu, F. Zhang, J. G. Huang, Y. Q. Gao, J. H. Chu, Sci. Rep. **5**, 10899 (2015).

[8] M. Vakiv, O. Shpotyuk, O. Mrooz, I. Hadzaman, J. Eur. Ceram. Soc. **21**(10), 1783 (2001).

[9] C. Ma, W. Ren, L. Wang, J. B. Xu, A. M. Chang, L. Bian, J. Eur. Ceram. Soc. **36**(16), 4059 (2016).

[10] Y. Hou, Z. M. Huang, Y. Q. Gao, Y. Ge, J. Wu, J. H. Chu, Appl. Phys. Lett. **92**(20), 147 (2008).

[11] R. Dannenberg, S. Baliga, R. J. Gambino, A. H. King, A. P. Doctor, J. Appl. Phys. **86**(5), 2590 (1999).

[12] C. Ma, H. G. Wang, P. J. Zhao, J. B. Xu, A.M. Chang, L. Wang, L. Bian, Mater. Lett. **136**, 225 (2014).

[13] C. Ma, W. Ren, L. Wang, L. Bian, J. B. Xu, A. M.

Chang, Mater. Lett. **153**, 162 (2015).
[14] Y. Q. Gao, Z. M. Huang, Y. Hou, J. Wu, Y. J. Ge, J. H. Chu, Appl. Phys. Lett. **94**(1), 1114 (2009).
[15] W. Zhou, J. Wu, C. Ouyang, Y. Q. Gao, X. Xu, Z. M. Huang, J. Appl. Phys. **115**, 093512 (2014).
[16] Z. G. Hu, X. J. Meng, Z. M. Huang, G. Wang, Q. Zhao, J. H. Chu, Jap. J. Appl. Phys. **42**(11), 7045 (2003).
[17] T. H. A. W. Brinkman, J. Mater. Res. **7**(5), 1278 (1992).
[18] W. Wei, W. Chen, D. G. Ivey, Chem. Mater. **20**(5), 1941 (2008).
[19] J. F. Marco, J. R. Gancedo, M. Gracia, J. L. Gautier, E. I. Ríos, H. M. Palmer, C. Greaves, F. J. Berry, J. Mater. Chem. **11**(12), 3087 (2001).
[20] A. Caballero, M. Cruz, L. Hernán, M. Melero, J. Morales, E. R. G. Castellón, J. Electrochem. Soc. **152**(3), A552 (2005).
[21] G. Hodes, "Chemical solution deposition of semiconductor films", Marcel Dekker, New York, 37-49 (2002).
[22] R. W. Schwartz, T. Schneller, R. Waser, CR. Chim. **7**(5), 433 (2004).
[23] F. C. Romeijn, Philips Res. Rep. **8**(5), 321 (1953).
[24] G. E. Jellison, F. A. Modine, Appl. Phys. Lett. **69**(3), 371 (1996).
[25] H. Fujiwara, "Spectroscopic ellipsometry: principles and applications", John Wiley & Sons, Chichester 29-31 (2007).
[26] I. Aulika, A. Dejneka, S. Mergan, M. Crepaldi, L. Jastrabík, Q. Zhang, A. Bencan, M. Kosec, V. Zauls, "Compositional and optical gradient in films of $PbZr_xTi_{1-x}O_3$ (PZT) family", InTech, Rijeka 579-602 (2011).
[27] A. Deineka, L. Jastrabik, G. Suchaneck, G. Gerlach, Phys. Status Solidi **188**(4), 1549 (2001).
[28] E. Weingartner, H. Saathoff, M. Schnaiter, N. Streit, B. Bitnar, U. Baltensperger, J. Aerosol Sci. **34**(10), 1445 (2003).
[29] W. B. Dai, Y. F. Lei, J. Zhou, Y. Zhao, Y. H. Zheng, M. Xu, S. L. Wang, F. Shen, J. Am. Ceram. Soc. **100**(11), 5174 (2017).
[30] Y. Q. Gao, Z. M. Huang, Y. Hou, J. Wu, W. Zhou, L. B. Zhang, J. H. Chu, Appl. Phys. A **114**(3), 829 (2013).

*Corresponding author: chaoma@yahoo.com